Journal of Advanced Ceramics
2024, **13**(12): 1919–1930
https://doi.org/10.26599/JAC.2024.9220988

Review

Extreme sputtering: Epitaxy of multifunctional oxides heterostructures

Soo Young Jung[1,2], Dong-Hun Han[1,2], Ruiguang Ning[1,3], Min-Seok Kim[1,2], Hyung-Jin Choi[1], Ho Won Jang[2,4], Seung-Hyub Baek[1,3]✉

[1] *Electronic Materials Research Center, Korea Institute of Science and Technology (KIST), Seoul 02792, Republic of Korea*
[2] *Department of Materials Science and Engineering, Research Institute of Advanced Materials, Seoul National University, Seoul 08826, Republic of Korea*
[3] *Division of Nano & Information Technology, KIST School, University of Science and Technology, Seoul 02792, Republic of Korea*
[4] *Advanced Institute of Convergence Technology, Seoul National University, Suwon 16229, Republic of Korea*

Received: July 23, 2024; Revised: September 24, 2024; Accepted: October 16, 2024

Abstract: This review provides an in-depth exploration of low-damage sputtering techniques and their importance in synthesizing high-quality epitaxial multifunctional oxide heterostructures. This review examines the factors contributing to damages during sputtering and introduces strategies for minimizing these detrimental effects. Prominent examples are provided to illustrate key milestones in the development of the sputtering technique, addressing critical issues such as maintaining stoichiometry when volatile species are included, achieving precise atomic-level control of interfaces, integrating an additional anion into oxides, selecting a particular phase from many possible polymorphs, and controlling the microstructure of thin films. Additionally, various defect mitigation strategies are discussed, including the use of miscut substrates, *in-situ* monitoring systems, and chemical buffer layers. By shedding light on the advancements and limitations in sputtering, this review not only enhances our present understanding of thin film deposition but also paves the way for future innovative sputtering techniques, holding tremendous potential for the exploration of new materials and their applications in various industries.

Keywords: sputtering; low damage; ion bombardment; epitaxial thin films; functional oxides

1 Introduction

Functional oxides exhibit a wide range of electrical, magnetic, and optical properties, covering almost all physical phenomena in condensed matter physics [1–3]. They include metallic conductors, ionic conductors, dielectrics, ferroelectrics, piezoelectrics, semiconductors, ferromagnetics, superconductors, nonlinear optics, and multiferroics. Owing to these diverse properties, functional oxides are used in electronics, optics, photo- or chemical-catalysts, energy storage and conversion, sensors and actuators, microelectromechanical systems, and quantum devices. Notably, they possess charge, spin, orbital, and lattice degrees of freedom, with their interplay giving rise to diverse properties. Functional oxide heterostructures serve as a fertile ground for exploring novel physics and chemistry, allowing manipulation of these degrees of freedom at the atomic scale through approaches such as strain engineering, domain engineering, cation and anion doping, and interface control. Through engineering of strain, interfaces, defects, and microstructures, researchers have been able to enhance material properties and unlock hidden functionalities [4–8]. However, despite brilliant academic achievements over the past three decades, no commercial devices utilizing epitaxial complex oxide heterostructures are currently available. To fully exploit their potential, it is necessary to employ industry-favorable thin film growth techniques.

✉ Corresponding author.
E-mail: shbaek77@kist.re.kr

Sputtering is a widely used technique to deposit thin films onto various substrates not only for fundamental research in the fields of materials science and engineering, physics, chemistry, and mechanical engineering, but also for industrial manufacturing in the fields of semiconductors, displays, optics, and solar cells [9–11]. The sputtering technique exhibits many beneficial features, offering precise film control, material versatility, high-quality coatings, and efficient production processes. Sputtering enables precise control over film thickness, composition, and functional properties of deposited materials. By manipulating process parameters such as plasma power, sputtering time, working pressure and target–substrate distance, manufacturers can achieve films with a wide range of physical properties, ensuring consistency and reproducibility in large-scale production. A wide range of materials, including metals, semiconductors, and insulators, can be used [12]. This versatility enables the deposition of diverse films, including multi-stacking, heterogeneous thin film structures, such as conductive metal layers, dielectric coatings, or optical films. Sputtered films exhibit high quality and uniformity across large areas: the directionality of the sputtering process helps achieve uniform film deposition, ensuring consistent performance across substrates. The sputtering-grown thin films are dense and strongly adherent to a substrate [13,14].

"Momentum transfer" is the key word used to describe the characteristics of sputtering technique. Sputtering involves physical bombardment of a target material with energetic ions to eject atoms or molecules from the target surface. These ejected

species are transported through a vacuum chamber and subsequently solidify onto a substrate. The bombarding ions are typically generated from the plasma of inert gases such as helium (He), neon (Ne), argon (Ar), and krypton (Kr) [15,16]. Argon plasma sputtering is widely employed due to the cost-effectiveness of argon gas, which is notably lower than that of other inert gases, such as Ne and Kr, along with a reasonably high sputtering yield. As a physical vapor deposition (PVD) technique, sputtering is especially beneficial for growing complex compounds, as it generally preserves the nominal composition of the target material in thin films.

Since the discovery of sputtering phenomenon by Sir William Grove in 1852 [17], several milestones [18–20] have been identified, as depicted in Fig. 1. Magnetron sputtering is designed to increase the deposition rate of thin films. In magnetron sputtering, the magnetic field from permanent magnets below a target creates closed electron orbits near the target surface by Lorentz force, confining the electrons and increasing their path length. Compared with traditional planar sputtering, this magnetic trapping of electrons near the target surface improves the ionization of gas atoms, producing a denser plasma with a higher ion density. This high density of ions leads to a high sputtering yield, resulting in a very fast deposition rate, as needed by manufacturing industries. Radio frequency (RF) sputtering was invented to deposit insulating materials. In RF sputtering, a high-frequency electrical power source, typically operating at a specific radio frequency of 13.56 MHz, is applied to the sputtering system. An insulating material cannot be sputtered by a traditional direct current (DC) sputtering technique because of electrical charging. The applied alternating current (AC) electric field can eliminate the electrical charging effect on the insulating target surface and create a persistent negative potential, so-called DC self-bias [21,22], at the capacitively coupled cathode (target), enabling sputtering by attracting positive ions. This self-bias originates from the large difference in mobility between positive ions and negative electrons in the plasma. Since only electrically conductive materials can be sputtered using DC sputtering, the RF sputtering technique expands the range of sputterable materials to include non-conductive materials. Similarly, pulsed DC sputtering can be employed, where a positive reverse bias is applied between the negative pulses to neutralize any accumulated charge on the surface of the insulating target. Reactive sputtering was invented to deposit compound materials such as oxides [23,24], nitrides [25,26], oxynitrides [27,28], and carbides [29,30]. In reactive sputtering, a reactive gas, such as oxygen or nitrogen, is introduced into the chamber during sputtering along with an inert sputtering gas. The interaction between the reactive gas and the sputtered species leads to chemical reactions, resulting in the formation of a compound different from the target material. For example, AlN thin films can be deposited by sputtering on an aluminum (Al) metal target with a flow of reactive nitrogen gas [31]. The reaction kinetics can be controlled by adjusting the deposition parameters, such as the partial pressure of reactive gas and sputtering power. When a reactive gas is introduced during reactive sputtering, chemical reactions can occur on the target surface. This can result in the accumulation of unwanted reaction byproducts, a phenomenon often referred to as target poisoning. Target poisoning can adversely affect the sputtering process by altering the composition of target material and impacting the quality of deposited thin films. Therefore, careful optimization of process parameters is essential to consistently grow thin films with the desired characteristics.

Nevertheless, in specific instances, the fundamental principle of sputtering—utilizing ionic bombardment for ejecting target materials through momentum transfer—proves detrimental for depositing desired high-quality thin films. The kinetic energy of the deposition flux during sputtering is notably high, ranging from a few electron volts (eV) to several tens of electron volts, which is a direct result of the momentum transfer mechanism [32,33]. Although the high kinetic energy of the sputtering deposition flux is advantageous for growing highly dense and strongly adherent thin films onto substrates, it can occasionally lead to both physical (atomic displacements, lattice defects, and surface roughening) and chemical (compositional changes and interdiffusion/intermixing) damage to the films. This, in turn, can impede the growth of high-quality single-crystal thin films. In this review, we delve into (1) the advancements in sputtering techniques designed to alleviate damages caused by highly energetic fluxes onto a substrate and (2) several examples of high-quality epitaxial thin films grown through sputtering, highlighting their superior physical properties.

2 Mechanism of sputtering damage

A plasma is a partially ionized gas consisting of equal numbers of positive ions and negative electrons, along with various unionized molecules, making the plasma electrically neutral. Despite the low population of charges in a plasma (typically ~10^{-4}), it behaves distinctly from normal gas. In a plasma, any solid surface, such as a wall or an electrode, which comes into contact with the plasma develops a sheath—a thin transition layer where plasma properties undergo abrupt changes from the bulk plasma to the solid surface [34]. The sheath region is depleted of free electrons due to their higher mobility than that of positive ions. As a result, the sheath region is dominated by positively charged ions and has a net positive space charge. The presence of net positive charge within the sheath region creates an electric field that accelerates positive charges towards the surface and repels negative charges. In the sputtering technique, there are two important sheaths: (1) a cathode sheath near the target on a sputtering gun and (2) an

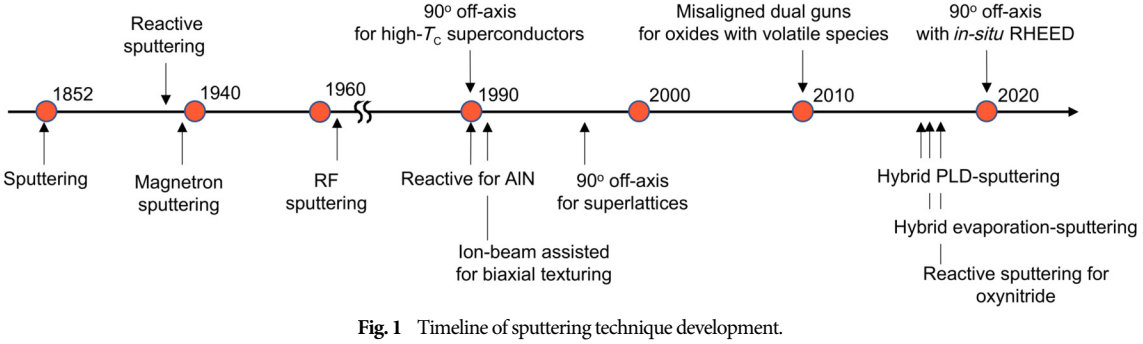

Fig. 1 Timeline of sputtering technique development.

anode sheath near the substrate. As shown in Fig. 2, a substantial voltage drop occurs near the cathode due to the applied negative DC bias in DC sputtering or DC self-bias in RF sputtering, resulting in the attraction of positive Ar ions toward the sputtering target positioned on the cathode. In contrast, a small voltage drop occurs near the grounded anode. The sputtering damage problem has to be understood as a bombardment of energetic particles under these electric potential boundary conditions in the plasma [35,36].

Figure 2 is a schematic illustration showing possible energetic particles that can damage the growing thin films on the substrate. First, the sputtered atoms ejected from the target possess a kinetic energy in the range of 1–10 eV, varying based on the binding energy of the target material; this elevated kinetic energy results from the momentum transfer of energetic Ar ions bombardment to the ejected atoms. The kinetic energy of the deposition flux in sputtering surpasses that in a thermal evaporator by more than one order of magnitude [37,38]; for example, copper atoms sputtered by 300 eV Ar^+ ions have a kinetic energy of approximately 2 eV, whereas thermally evaporated copper atoms at 1300 K have a kinetic energy of only approximately 0.1 eV. Second, Ar^+ ions or neutralized Ar atoms reflected from the target possess a kinetic energy of approximately 15 eV. These energetic ions can move toward the substrate after bouncing back from the target surface. Once these backscattered ions undergo neutralization, they can retain their high kinetic energy without being influenced by the cathode potential, potentially causing damage to the growing film on the substrate. Third, positive ions near the anode can be accelerated towards the substrate along the anode potential gradient. Their kinetic energy is approximately 15 eV, which is still high enough to influence the quality of growing thin films. For comparison, notably, the kinetic energy of Ar^+ ions bombarding the target along the cathode potential gradient ranges from 100 to 1000 eV. Fourth, negative ions, which are repelled from the substantial negative potential of the cathode, have the potential to damage the growing film on the substrate. Oxygen frequently acts as the primary source of negative ions during the sputtering growth of oxide thin films. When negative ions primarily originate from the carrier gas in the plasma, their kinetic energy ranges from approximately 5 to 15 eV. However, if they are formed near the target, they can experience acceleration due to the large negative cathode potential, leading to an increase in their kinetic energy up to ~400 eV. Notably, oxygen-negative ions play a crucial role as a species that detrimentally influence the quality of oxide thin films.

3 Off-axis configuration for low damage sputtering

Off-axis sputtering is a technique used to minimize damage to thin films caused by energetic particle bombardment. In this method, the target and substrate are positioned at an angle rather than in the conventional face-to-face alignment. Most high-energy particles travel in a straight line perpendicular to the target surface, so by positioning the substrate off-axis, the impact of these particles on the growing film is reduced. However, this strategy may lower the growth rate and affect the thickness uniformity across the substrate. There are two distinct off-axis configurations: (1) 90° off-axis sputtering [39–41] and (2) misaligned dual gun sputtering [42], as shown in Fig. 3. While the off-axis geometry facilitates the growth of high-quality epitaxial oxide thin films, it presents challenges related to deposition rate and uniformity. Misaligned dual gun sputtering was specifically developed to address the slow deposition rates associated with 90° off-axis sputtering. By rotating the substrate during deposition, the uniformity can be improved, ensuring a more even material distribution across the surface.

A common configuration for off-axis sputtering is the 90° off-axis setup, where the angle between the target and substrate

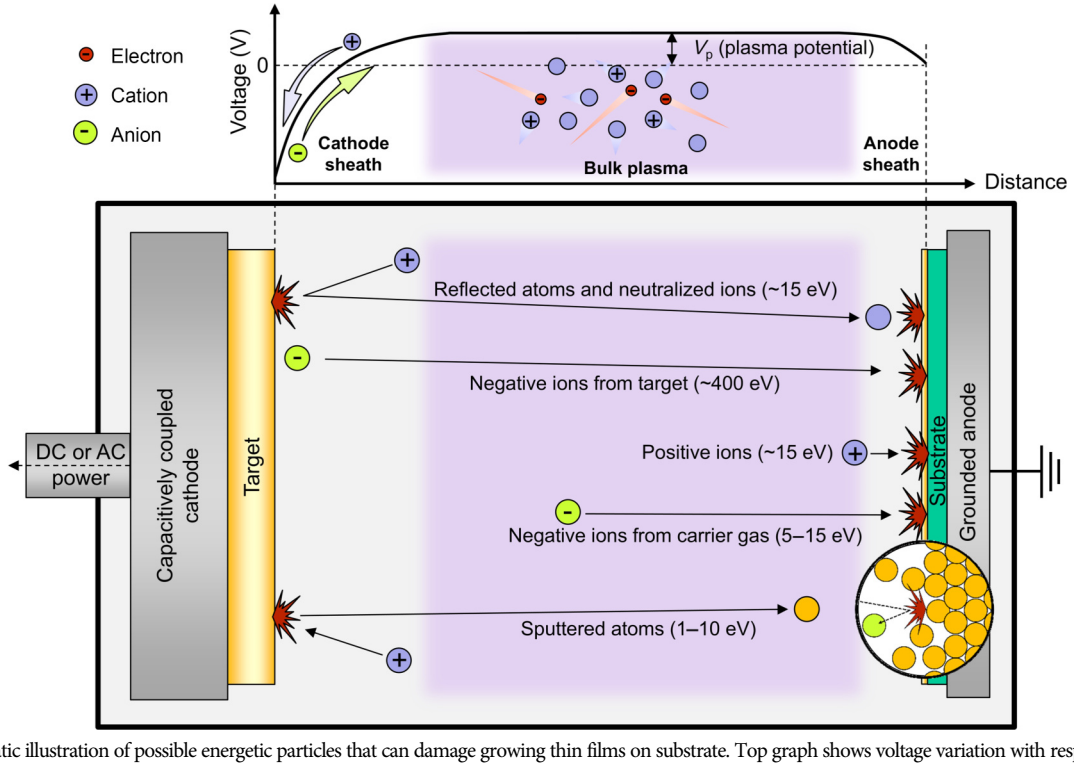

Fig. 2 Schematic illustration of possible energetic particles that can damage growing thin films on substrate. Top graph shows voltage variation with respect to distance between target and substrate.

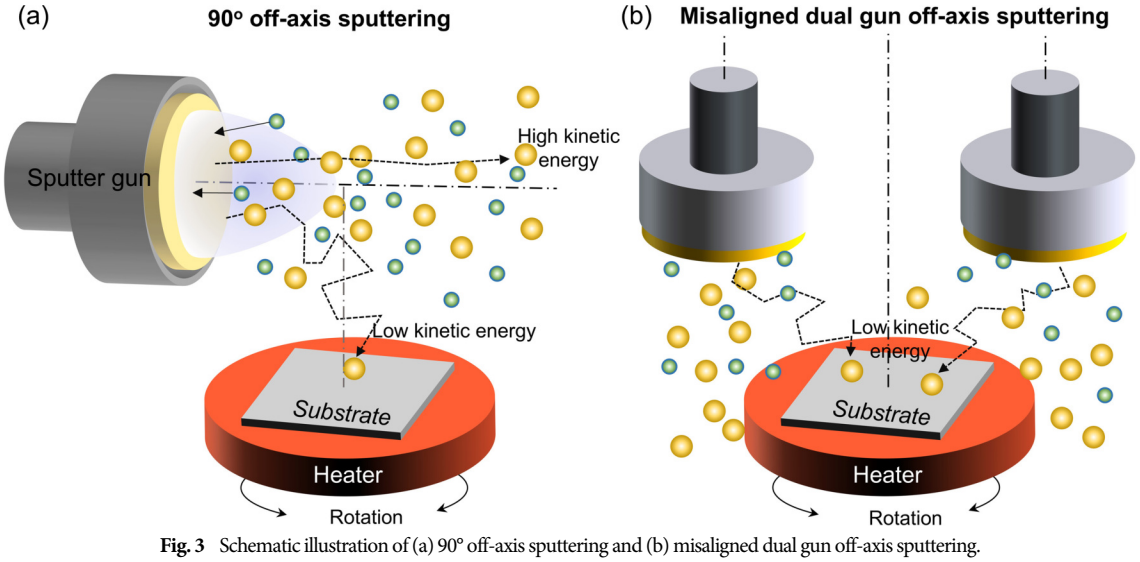

Fig. 3 Schematic illustration of (a) 90° off-axis sputtering and (b) misaligned dual gun off-axis sputtering.

normals is perpendicular (Fig. 3(a)). This configuration is highly effective in preventing highly energetic particles from traveling directly in a straight path from the target. In 90° off-axis sputtering, the typical working pressure is considerably high, often reaching several hundred millitorrs, in contrast to conventional sputtering methods, which typically operate with a few millitorrs. The elevated working pressure facilitates effective scattering, leading to a reduction in the kinetic energy of the deposition flux. At a pressure of 200 mTorr, the mean free path of Ar gas is approximately 0.3 mm [43], indicating that collisions between gas particles frequently occur before the sputtered atoms reach the substrate. Additionally, the high working pressure contributes to an increased deposition flux toward the substrate by facilitating the diffusion of sputtered atoms through scattering processes. Therefore, 90° off-axis sputtering technique is commonly employed for fabricating high-quality epitaxial oxide heterostructures, which utilize a low-energy deposition flux.

Misaligned dual gun sputtering configuration is another type of off-axis sputtering, where two parallel sputtering guns are positioned on-axis with the substrate between them, as shown in Fig. 3(b). Aligning the substrate heater with parallel sputter guns enables a faster deposition rate than 90° off-axis sputtering, and rotating the substrate heater enhances film uniformity over a broader substrate area [42]. A high working pressure is necessary to mitigate the kinetic energy of energetic particles and to diffuse the deposition flux laterally. This geometry not only minimizes sputtering damages from energetic particles but also increases the deposition rate. The rapid deposition rate often helps maintain the chemical composition of thin films, particularly when the target material includes volatile species such as PbO and Bi_2O_3, by suppressing their re-evaporation at high growth temperatures.

4 Epitaxial growth of oxide heterostructures by sputtering

4.1 Oxides including volatile elements $Pb(Mg,Nb)O_3$–$PbTiO_3$ (PMN–PT) and $BiFeO_3$

Depositing compound materials containing volatile elements is one of the most challenging aspects in the thin-film deposition process. Typically, the substrate is heated during thin film growth to form a crystalline phase with fewer defects by increasing the mobility of atoms and molecules. For the epitaxial thin film growth of complex oxides, the typical substrate temperatures range from 500 to 800 °C. Volatile elements can re-evaporate from the substrate at these temperatures. There are several volatile binary oxides: Li_2O, K_2O, Na_2O, V_2O_5, Bi_2O_3, and PbO. Owing to the relatively high volatility of these elements, it is challenging to synthesize stoichiometric, phase-pure, epitaxial thin films of compounds containing them such as $LiNbO_3$, $LiTaO_3$, $KTaO_3$, $(K,Na)NbO_3$, $BiVO_3$, $BiFeO_3$, and PMN–PT; non-stoichiometric thin films and unwanted secondary phases are easily formed. These defects can affect the physical properties of thin films; for example, an insulating material becomes electrically leaky, and dielectric properties are deteriorated. To compensate for the loss of volatile elements, sputtering targets, including an excessive amount of volatile substances, have been employed [44,45]. Another approach is to use miscut substrates with vicinal surfaces, where the crystal planes are cut slightly from a high-symmetry direction [46,47]. This method leverages the high reactivity of step edges on the vicinal surface of miscut substrates. The step edges, as preferential nucleation sites, can fix volatile elements from re-evaporation [48]. Here, we present two examples of successful growth of epitaxial PMN–PT and $BiFeO_3$ thin films that contain volatile PbO and Bi_2O_3 species, respectively, using sputtering techniques.

A PMN–PT single crystal, which represents a relaxor-ferroelectric solid solution, is renowned for its superior piezoelectric response compared with that of conventional piezoelectric materials such as $Pb(Zr,Ti)O_3$ (PZT). To apply this piezoelectric material in microelectromechanical systems (MEMSs) with highest efficiency, Baek *et al.* [49] deposited an epitaxial PMN–PT layer on a silicon substrate with $SrRuO_3/SrTiO_3$ buffer layers. The major challenge was to grow perovskite phase-pure thin films without any non-piezoelectric, pyrochlore secondary phases that can easily form through the loss of PbO. The key technique to obtain epitaxial phase-pure PMN–PT thin films was to use a misaligned dual-gun sputtering system and a miscut Si substrate. Figure 4(a) shows θ–2θ scan of 3.5-μm-thick PMN–PT film grown on 4° miscut Si substrate, indicating the pure perovskite epitaxial state of the film. The azimuthal φ scan measurement (Fig. 4(b), where φ represents the in-plane rotational angle of the sample during the XRD measurement) shows in-plane epitaxy of PMN–PT film, which has 45° in-plane rotation with respect to the Si substrate. Transition electron microscopy (TEM) analyses (Figs. 4(c) and 4(d))

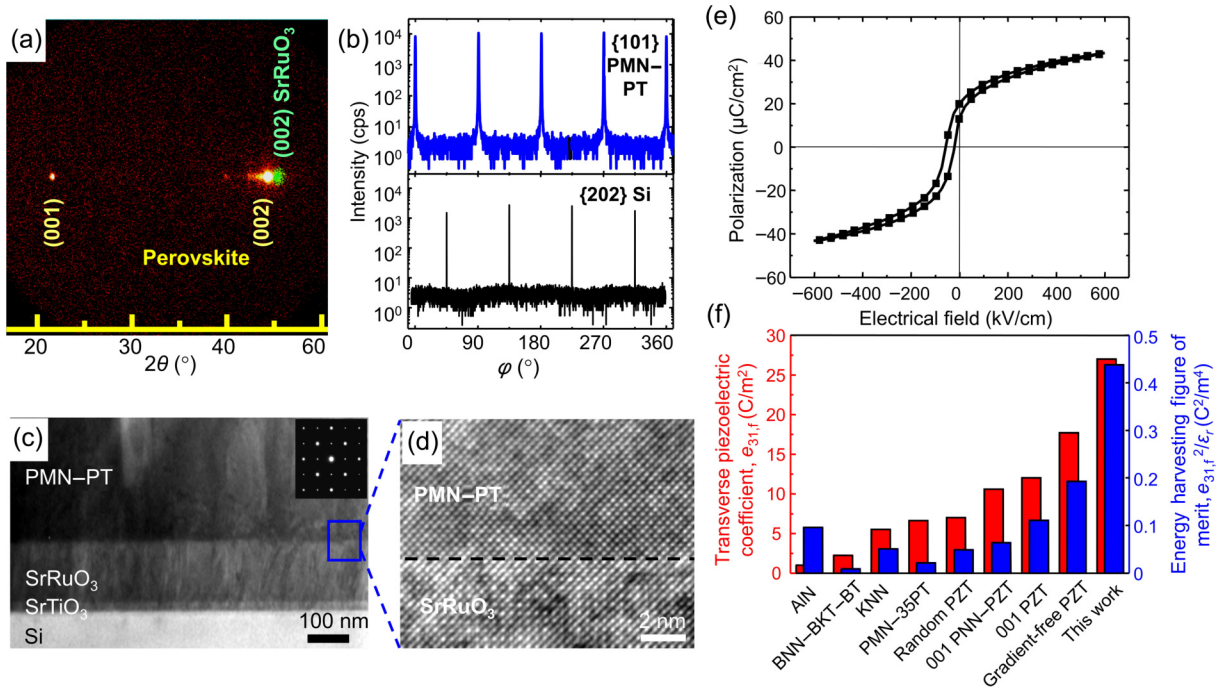

Fig. 4 (a) X-ray diffraction pattern measured with 2D area detector of PMN–PT heterostructure on Si(001) substrate with 4° miscut along [110]. (b) φ scan of $(101)_{pc}$ PMN–PT (pc, pseudocubic) and (202) Si diffraction peaks. (c) Bright-field cross-sectional TEM image near the interface between PMN–PT and $SrRuO_3$, with the inset of SAED image of PMN–PT along [100] zone axis. (d) High-resolution TEM image of PMN–PT and $SrRuO_3$ interface. (e) *P–E* curve of 1-μm PMN–PT thin film on Si. (f) Comparison of figure of merit of micromachined actuators ($e_{31,f}$) and energy harvesters ($e^2_{31,f}/\varepsilon_0\varepsilon_{33}$) of a PMN–PT film from this work with other reported values. Reproduced with permission from Ref. [49], © The American Association for the Advancement of Science 2011.

also confirmed cube-on-cube epitaxial relationship between PMN–PT and $SrRuO_3$ on Si. The polarization–electric field (*P–E*) curve of 1-μm-thick PMN-PT film on Si shows a ferroelectric imprint, a lateral shift in the *P–E* curve, along the negative direction beyond its coercive field (Fig. 4(e)). The piezoelectric constant $e_{31,f}$ determined by the wafer flexure method [50] is approximately −27 C/m² (Fig. 4(f)).

Multiferroic $BiFeO_3$ exhibits ferroelectricity, ferroelasticity, and anti-ferromagnetism, simultaneously. In the early days, the growth of $BiFeO_3$ thin films often resulted in Fe_2O_3 secondary phases due to the loss of volatile Bi_2O_3. Moreover, the ferroelectric switching path and dynamics of [111] polarization in the rhombohedral $BiFeO_3$ unit cell were obscure. Baek *et al.* [51] were able to grow high-quality, phase-pure epitaxial $BiFeO_3$ thin films using a misaligned dual gun sputtering system and a miscut $SrTiO_3$ substrate. Utilizing a 4°-miscut $SrTiO_3$ substrate along the [110] direction not only aids in fixing volatile Bi_2O_3 to achieve stoichiometric, phase-pure thin films but also enhances the ferroelectric properties by forming a monodomain $BiFeO_3$ structure. The step-and-terrace structure on the surface of miscut substrates breaks the four-fold symmetry of the (001) plane of cubic STO substrates. Such symmetry breaking can select preferential domains among four possible domains [52,53].

A 600 nm-thick, epitaxial $BiFeO_3$ thin film on a 4°-miscut $SrTiO_3$ substrate along the [110] direction shows an atomically smooth surface with a step and terrace structure (Fig. 5(a)). The structure of $BiFeO_3$ mono-domain was confirmed by X-ray diffraction (XRD) reciprocal space mapping (RSM) of $(\bar{1}03)$ peak (Fig. 5(b)) and cross-sectional TEM analysis (Fig. 5(c)). The polarization direction of the as-grown $BiFeO_3$ thin films was confirmed to be downward from the *P–E* measurement of a virgin capacitor (Fig. 5(d)). The $SrRuO_3$ bottom electrode allows screening of the depolarization field by the free charges present in the electrode. This screening effect leads to the stabilization of ferroelectric mono-domain state. Note that the *P–E* hysteresis loop has a square-like shape with closed ends, indicating that the $BiFeO_3$ film is highly insulating and less defective (inset of Fig. 5(d)). Some domain boundaries in insulating ferroelectrics become electrically conducting due to the modification of atomic bonds at the boundaries [54,55]. The highly insulating and excellent ferroelectric properties of mono-domain $BiFeO_3$ thin films mainly originate from the absence of defective domain boundaries. Out-of-plane and in-plane piezoresponse force microscopy (PFM) analyses also confirm that the $BiFeO_3$ thin film on the 4° miscut $SrTiO_3$ substrate along [110] direction has a mono-domain structure (Fig. 5(e)). Using these high-quality, simple monodomain $BiFeO_3$ thin films, preferential ferroelectric switching paths, retention, and cycling endurance were discovered [51,56].

Since two sputtering guns operate simultaneously in the misaligned dual gun sputtering system, it is important to avoid any electric or magnetic interaction between them. Brewer *et al.* [42] reported that substrate rotation in a misaligned dual gun sputtering system enabled large-scale uniformity in terms of thickness, composition, and ferroelectric properties. The deposition rate of PMN–PT thin films is relatively low at approximately 0.1 μm/h [42,49]. Additional investigations of sputtering process parameters will be necessary to enhance the deposition rate to a commercially viable level.

4.2 Superlattices: $PbTiO_3/SrTiO_3$

A superlattice is a periodic solid structure composed of alternating nanometer-sized layers of two or more different materials. This artificial structure provides an excellent platform to explore novel physics arising not only from the combination of physical properties from each layer, but also from strain modulation and interfacial effects. Several studies have been conducted to control properties such as dielectric constant, thermal conductivity, and

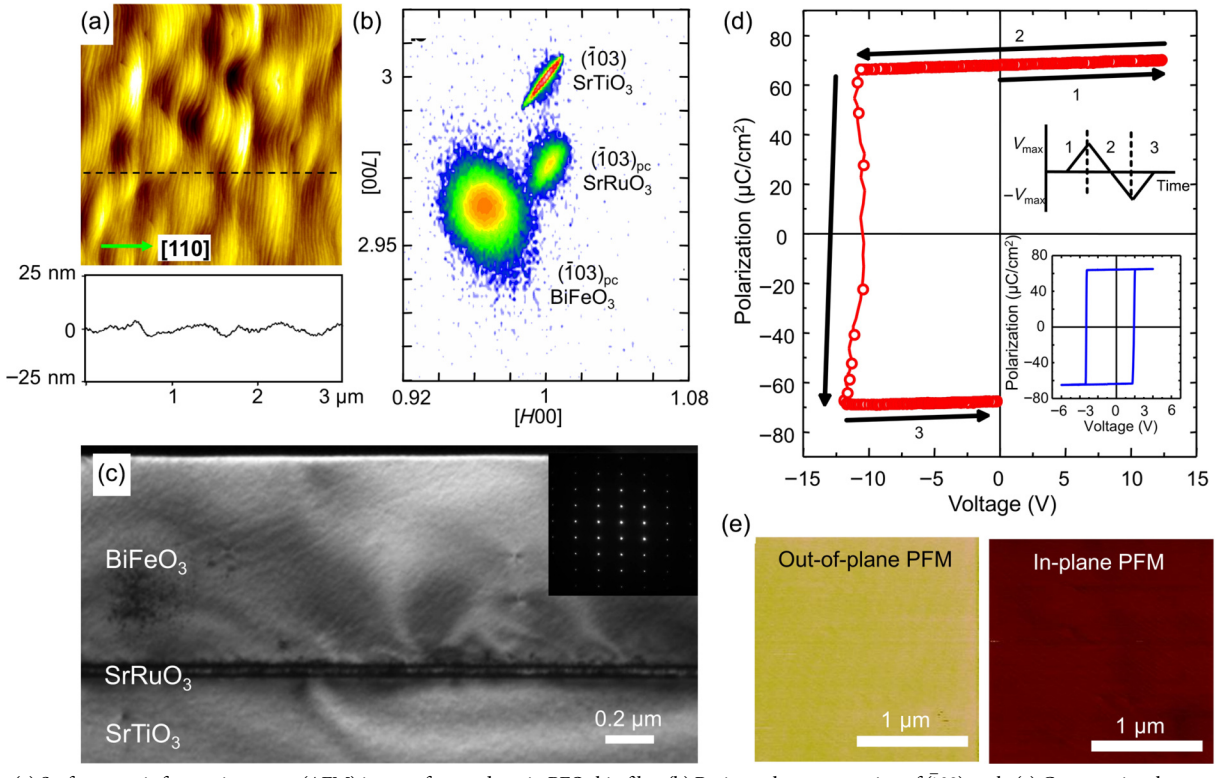

Fig. 5 (a) Surface atomic force microscopy (AFM) image of monodomain BFO thin film. (b) Reciprocal space mapping of (1̄03) peak. (c) Cross-sectional transmission electron microscopy image of $BiFeO_3/SrRuO_3/SrTiO_3$, with the inset of selected-area electron diffraction (SAED) image of $BiFeO_3$ region. (d) Virgin measurement of *P*–*E* loop, with the top inset of profile of applied voltage during *P*–*E* loop measurement as a function of time, and bottom inset of *P*–*E* loop of the following measurement. (e) Out-of-plane and in-plane PFM image on as-grown mono-domain $BiFeO_3$ films. Reproduced with permission from Ref. [51], © Springer Nature Ltd. 2010.

band gap [57–61]. However, the synthesis of high-quality epitaxial oxide superlattices is a challenging task, requiring impeccably clean interfaces between its layers, devoid of intermixing, and demanding precise modulation of thickness at the atomic layer level. For this purpose, molecular beam epitaxy (MBE) or pulsed laser deposition (PLD) techniques are commonly used in the synthesis of epitaxial oxide superlattices, leveraging their ability to precisely control the thickness of each layer through techniques such as reflection high energy electron diffraction (RHEED) [59,61,62]. Here, we introduce a study of epitaxial $PbTiO_3/SrTiO_3$ superlattice fabricated by a sputtering technique.

Dawber *et al.* [63] deposited epitaxial superlattices consisting of $PbTiO_3$ and $SrTiO_3$using 90° off-axis magnetron sputtering on Nb-doped $SrTiO_3$ substrates. They employed constituent layer thickness ratio as a tuning parameter for controlling electronic properties. θ–2θ XRD scan of 2-unit cell $PbTiO_3$/5-unit cell $SrTiO_3$×36 superlattice shows satellite peaks originating from the periodicity of $PbTiO_3$ and $SrTiO_3$ layers. The full width at half maximum (FWHM) of (001) rocking curve is 0.066°, which is indicative of high crystallinity. Reciprocal space mapping of (114) peak shows that all the $PbTiO_3$ and $SrTiO_3$ layers are coherently grown. The AFM image shows an atomically smooth surface of superlattice with a step and terrace structure. The polarization–voltage curves of superlattices with different ratios of constituent layers demonstrate the ability to systematically adjust the polarization in a predictable manner across the range from 0 to 60 μC/cm² by varying the $PbTiO_3$ volume fraction within the range of 0.4–1. Moreover, the ferroelectric transition temperature (T_C) can be adjusted within the range from 500 to 800 K by manipulating the composition of the superlattice through strain engineering.

This work reveals that the 90° off-axis sputtering technique enables the growth of high-quality epitaxial oxide superlattices. When multiple sputtering guns are installed for growing superlattices, the sputtering chamber should be carefully designed to prevent any magnetic interference between the magnetron sputtering guns and potential cross-contamination between targets. A shutter positioned in front of each sputtering gun can be utilized to shield both the deposition flux and magnetic field from neighboring guns. However, when multiple guns are installed for 90° off-axis sputtering, the chamber may not be spacious. One potential solution involves making the sputtering gun movable through linear motion feedthroughs, allowing for the push-pull motion of sputtering guns. In this work [63], superlattice samples were fabricated without reflection high-energy electron diffraction (RHEED). The absence of *in-situ* thickness monitoring equipment with a resolution down to the unit-cell thickness may cause non-uniform interfaces as the number of layers increases. The integration of RHEED system with sputtering will be discussed later.

4.3 *In-situ* RHEED monitoring: $SrRuO_3$

Interfaces at epitaxial oxide heterostructures provide excellent platforms for exploring emergent phenomena. When materials with distinct properties are brought together, entirely new behaviors can emerge at the interface that do not exist in either material alone. One remarkable example is the interface between two insulating materials, $LaAlO_3$ and $SrTiO_3$, where a two-dimensional electron gas (2DEG) forms. This 2DEG displays both superconductivity and the unusual coexistence of superconductivity and ferromagnetism [64–66]. To investigate these interfaces effectively, precise control of thin-film growth at the atomic level is imperative.

RHEED is a versatile tool that is capable of both probing the

crystallography of a solid's surface and providing high-resolution thickness monitoring of growing films at the unit-cell level. RHEED systems are commonly integrated into most MBE and PLD setups to enable precise control over film thickness and interface termination. Since this technique relies on electron diffraction it is crucial to maintain a magnetism-free environment near the substrate. Therefore, the substrate heater should be powered using DC rather than AC, as it does not generate a field-induced magnetic field.

However, the characteristics of contemporary sputtering systems pose a challenge when integrating RHEED. At present, magnetron sputtering is the widely preferred method. It employs magnets positioned behind the target to focus electrons near the target surface, thereby enhancing the ionization of argon (Ar) gas and leading to improved deposition rates. The magnetic field generated by the magnetron sputtering gun deflects the electron beams away from the RHEED screen. To address this challenge, Podkaminer *et al.* [67] introduced a method to counteract the magnetic field when the RHEED system was integrated into magnetron sputtering setups. The magnetic field of the working gun was compensated by adding another identical gun to the opposite side, using an antisymmetric setup, as shown in Fig. 6(a). This research demonstrated the observation and control of $SrRuO_3$ deposition, which is a material widely used as an oxide electrode for epitaxial functional oxide deposition. Owing to the negligible bending of the electron beam path across the plasma and its reach to the phosphor screen, the RHEED intensity oscillation during $SrRuO_3$ growth was recorded, as shown in Fig. 6(b). AFM measurements of $SrTiO_3$ substrate (Fig. 6(c)) and deposited $SrRuO_3$ film (Fig. 6(d)) both show step terrace surfaces, indicating a typical $SrRuO_3$ layer-by-layer growth process. The out-of-plane θ–2θ scan, depicted in Fig. 6(e), exhibits Laue oscillations, thus confirming the presence of a remarkably smooth surface and well-defined interface. The omega rocking curve of the $SrRuO_3$ film, as illustrated in Fig. 6(f), demonstrates a full width at half-maximum (FWHM) value of 0.02°, indicating an exceptional degree of crystallinity. Note that epitaxial $SrRuO_3$ thin films are typically grown in the step-flow growth mode, where the film grows continuously laterally from step edges without nucleation occurring on terraces. When films grow in the step-flow growth mode, RHEED cannot be utilized for *in-situ* monitoring of the thickness of growing films; it is only applicable when films grow in the layer-by-layer growth mode. With the help of RHEED, it would be possible to grow epitaxial superlattices with more clean and well-defined interfaces.

4.4 Oxynitrides by reactive sputtering: SnON

Reactive sputtering involves introducing a reactive gas into the chamber to deposit compound thin films. Reactive gases, such as N_2 [68], O_2 [69,70], and CH_4 [71], interact with the sputtered pure atoms, resulting in the deposition of nitrides, oxides, and carbides, respectively, on the substrate. In particular, synthesizing an oxynitride, a chemical compound with both oxygen and nitrogen elements as constituent anions, is challenging. Oxygen and nitrogen exist in a gaseous state, making it challenging to precisely control the nominal composition of anions in a solid, in contrast to cations, which are predominantly solid. Furthermore, the substantial difference in reactivity between oxygen and nitrogen poses a challenge in achieving precise control over the oxygen-to-nitrogen ratio during the synthesis of oxynitride materials. Gwon *et al.* [72] successfully grew tin oxynitride (SnON) thin films using reactive sputtering techniques. The initial approach involved utilizing a Sn metal target with only N_2 flow as both sputtering and reactive gas. Remarkably, SnON thin films were created without the need for O_2 gas flow; the residual O_2 in the sputtering chamber (at a base pressure of ~10^{-5} Torr) was integrated into the growing film to form oxynitrides. Even the slightest introduction of O_2 gas resulted in the formation of SnO_2,

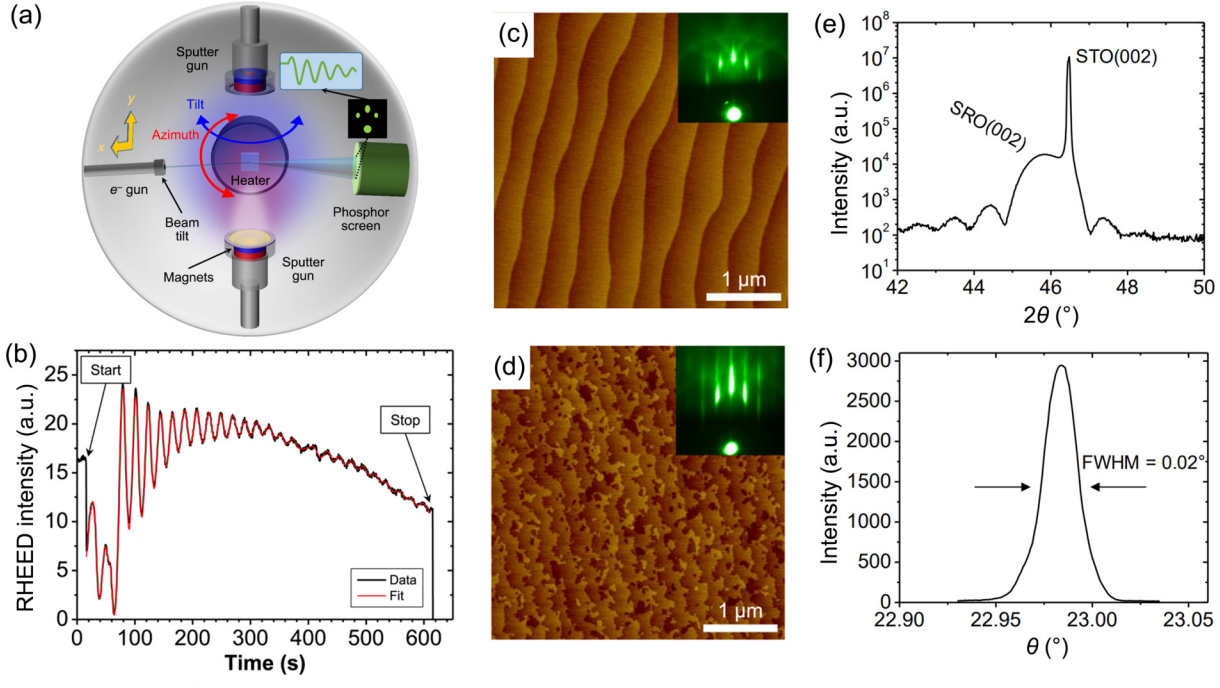

Fig. 6 (a) Schematic image of sputter chamber with RHEED setup. (b) Specular spot RHEED oscillations during $SrRuO_3$ growth on $SrTiO_3$. The actual data are black, with Gaussian fit in red. (c) AFM image of $SrTiO_3$ substrate prior to growth, with the inset of RHEED image of $SrTiO_3$ substrate in vacuum before growth. (d) AFM image of $SrRuO_3$ surface, with the inset of RHEED image of $SrRuO_3$ film after growth. (e) Out-of-plane θ–2θ line scan XRD of $SrRuO_3/SrTiO_3$. (f) Rocking curve of (002) $SrRuO_3$ thin film. Reproduced from Ref. [67], © Author(s) 2016.

excluding the incorporation of N atoms, which was attributed to the stronger reactivity of oxygen than that of nitrogen. Since this method depends on residual oxygen, it is not an appropriate approach for reproducibly growing SnON thin films with precise control over the O/N ratio. The second approach involves utilizing a SnO_2 oxide target. In this case, it is necessary to partially reduce the sputtered SnO_2 molecules into SnO_x and then incorporate N atoms to create SnON. Ammonia (NH_3) gas, which serves as both a reduction agent and a nitrogen source, was additionally introduced along with N_2 gas into the reactive sputtering chamber. This method offers extensive flexibility in controlling the O/N ratio through the adjustment of sputtering process parameters, in contrast to the first method.

Using the second approach, Gwon *et al.* [72] were able to grow epitaxial SnON thin films on MgO(001) single-crystal substrates, as shown in Fig. 7. The cube-on-cube epitaxial relationship between SnON and MgO was confirmed by out-of-plane XRD θ–2θ scan (Fig. 7(a)) and azimuthal XRD scan (Fig. 7(b)). The cross-sectional high-resolution TEM image (Fig. 7(c)) revealed that a high density of misfit dislocations existed at the SnON/MgO interface. This can explain how SnON thin films (cubic, a = 5.09 Å) can be epitaxially grown on MgO substrates (cubic, a = 4.12 Å), despite a substantial lattice mismatch of approximately 20%. The AFM image revealed that the epitaxial SnON film was atomically smooth, with a surface roughness within the range of two unit-cell heights, despite the film being 120 nm thick (Fig. 7(d)).

The composition of nitrogen was controlled solely by varying the sputtering power during deposition. As the sputtering power increases, the nitrogen content in SnON thin films increases, primarily due to the greater activation of NH_3 molecules, which serve as both a reduction agent and a nitrogen source. SnON films with various nitrogen contents were deposited on a glass substrate to determine the relationship between the film composition and its optical properties. As the sputtering power increased, the nitrogen content in the film increased, which caused a decrease in the optical transmittance (Fig. 7(e)). The Tauc model was applied to measure the optical band gap of the film. Figure 7(f) shows the plot of $\alpha h\nu^2$ vs. photon energy ($h\nu$) of SnON films with varying nitrogen compositions. With increasing nitrogen content, the optical band gap of SnON film decreased from 3.6 to 3.3 eV. The inset image shows that the film becomes increasingly opaque as the nitrogen content increases. These results highlight that a judicious selection of flowing gases, targets, and substrates in reactive sputtering techniques can yield epitaxial thin films that encompass a broad spectrum of compounds, including oxygen, nitrogen, sulphur, carbon, and various combinations of anions.

4.5 Phase selection and self-texturing: VO_2

Binary oxides display a wide range of physical properties stemming from their capacity to form diverse compounds and their polymorphs. For example, the existence of multiple types of vanadium oxides arises from the ability of vanadium to exhibit various oxidation states, ranging from +2 to +5, resulting in compounds such as VO, V_2O_3, VO_2, and V_2O_5. As a polymorphic material, each compound can possess multiple crystal structures. For example, VO_2 has three types of polymorphic structures: tetragonal, monoclinic A, and monoclinic B. Therefore, it is important to selectively synthesise the desired compound with a particular polymorph.

Textured microstructures often emerge in thin films, where a specific crystallographic direction of a material is aligned parallel to the out-of-plane direction, while exhibiting random orientations along the in-plane directions. Textured thin films play an important role in improving material properties by reducing the occurrence of defective grain boundaries and harnessing anisotropic properties for enhanced performance. For example, in magnetic tunnel junctions (MTJs), the MgO tunnel barrier layer

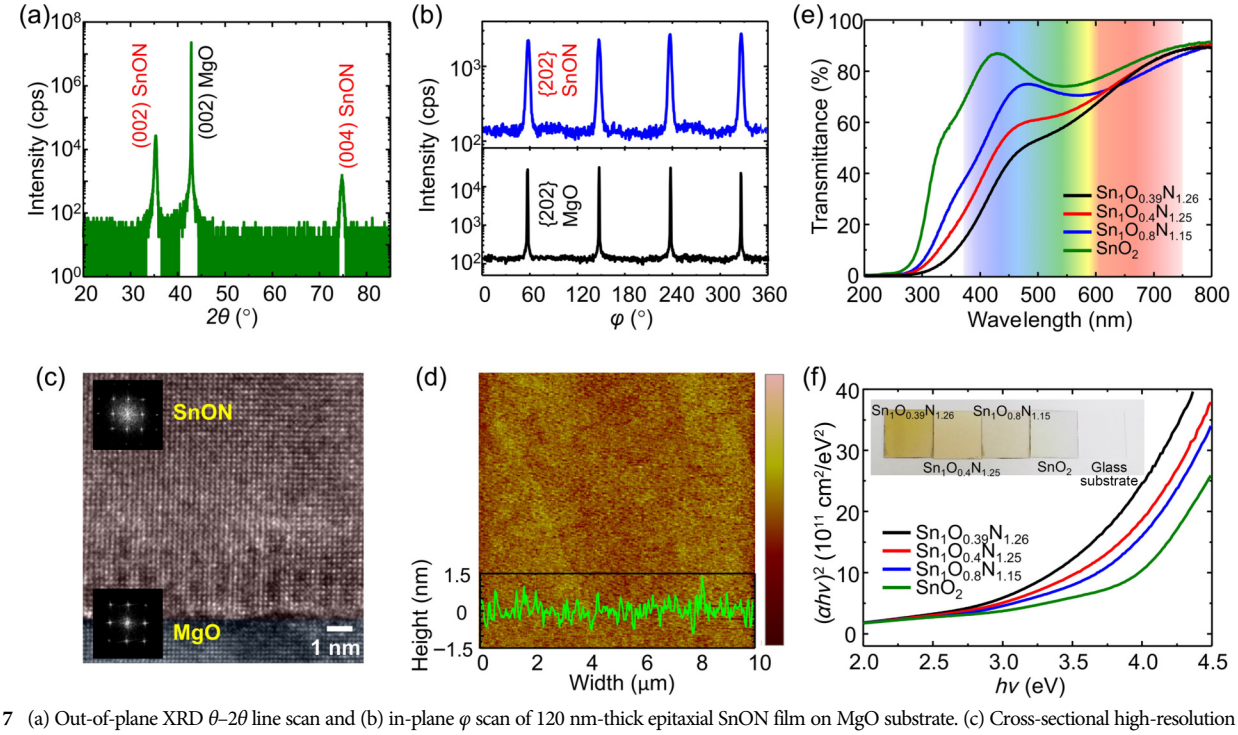

Fig. 7 (a) Out-of-plane XRD θ–2θ line scan and (b) in-plane φ scan of 120 nm-thick epitaxial SnON film on MgO substrate. (c) Cross-sectional high-resolution TEM image at SnON/MgO interface with a [100] zone axis, with the inset of fast Fourier transform pattern of SnON film and MgO substrate. (d) Surface morphology of epitaxial SnON film on MgO substrate. (e) Optical transmittance spectra and (f) plot of $\alpha h\nu^2$ vs. $h\nu$ of SnON films grown with different RF powers, with the inset of optical image of SnON films on glass substrates. Reproduced with permission from Ref. [72], © American Chemical Society 2016.

can be grown with a self-textured (001) orientation along the out-of-plane direction, enhancing its magnetoresistance performance and reliability. The primary mechanism driving self-texturing in thin films is the minimization of surface energy: certain crystallographic orientations may have lower surface energy than others, leading to preferential growth along those orientations.

The paper by Kil *et al.* [73] addresses both phase selection and self-texturing in VO_2(B) thin films. Notably, an amorphous $SrTiO_3$ buffer layer plays a critical role in the selective growth of VO_2(B) phase among many polymorphs, as well as in achieving (001) self-texturing along the out-of-plane direction. The $SrTiO_3$ buffer layer is grown by RF sputtering at room temperature under a pressure of 5 mTorr (Ar : O_2 = 80 : 20), which is an oxygen-deficient condition. Figures 8(a) and 8(b) show the X-ray diffraction patterns of the out-of-plane θ–2θ scans of the VO_2(B)/amorphous $SrTiO_3/SiO_2$/Si samples measured by a point detector and an area detector, respectively. These results indicate that the phase-pure, monoclinic VO_2(B) thin films are selectively grown on amorphous $SrTiO_3$ buffer layers under sputtering growth conditions, where other compounds such as V_2O_5 can be formed concurrently. Moreover, the XRD results show that VO_2(B) thin films are highly 00*l*-textured. From a conventional perspective, it is less likely for an amorphous layer to select a particular phase and form a textured microstructure, as the random atomic arrangement in the amorphous layer does not provide a structural template to accommodate 00*l*-oriented VO_2(B) thin films.

The cross-sectional TEM image of the VO_2(B)/amorphous $SrTiO_3/SiO_2$/Si heterostructure (Figs. 8(c)–8(e)) shows that a textured, crystalline VO interfacial layer with a thickness of < 5 nm is newly formed at the interface between the VO_2(B) film and the amorphous $SrTiO_3$ buffer layer. This layer acts as an "oxygen-absorbing sponge", reducing the deposition flux and promoting the formation of the VO interfacial layer. The $SrTiO_3$ buffer layer grown under oxygen-deficient conditions may possess a high density of oxygen vacancies, and the amorphous state allows for fast transport of oxygen vacancies. An additional benefit of using an amorphous buffer layer is the improvement in surface flatness. This chemically and structurally designed $SrTiO_3$ buffer layer can promote the formation of the VO interfacial layer by reducing the deposition flux. Once the oxygen is saturated in the amorphous $SrTiO_3$ buffer layer, the VO interfacial layer stops growing, and it acts as a phase-selective template for VO_2(B) thin films owing to its structural coherency, as depicted in Fig. 8(f). Note that the 12 unit cells of VO(001) plane are comparable to the 4 unit cells of VO_2(B)(001) plane. The 00*l*-texture of VO_2(B) films is also dictated by the 00*l*-texture of the VO interfacial layer. These effects of the amorphous buffer are not restricted to $SrTiO_3$; the amorphous $SrRuO_3$ and $LaAlO_3$ buffer layers play identical roles.

The highly textured (001) VO_2(B) thin films exhibit excellent physical properties for the high-temperature application of infrared imaging bolometers. The temperature coefficient of resistance (TCR) is high (> −3.5%/K at 25 °C and > −1.5%/K at 95 °C), and the electrical resistivity is low (~5×10^{-1} Ω·cm at 25 °C and < 1×10^{-1} Ω·cm at 95 °C). There is no hysteresis during temperature cycling. These characteristics are favorable for realizing highly sensitive, low-noise microbolometers operating at temperatures over 100 °C [74]. Moreover, the reproducibility of

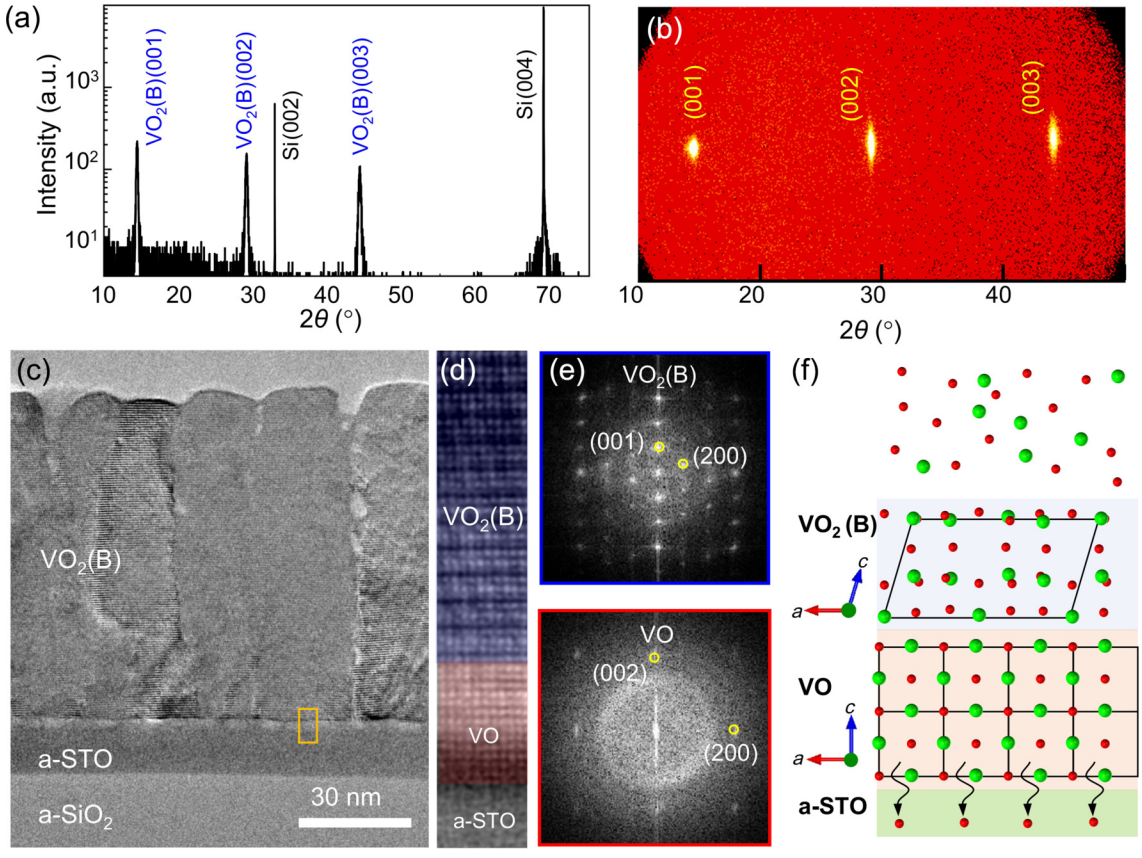

Fig. 8 Out-of-plane XRD θ–2θ line scan measured by (a) a point detector and (b) an area detector. (c) Cross-sectional TEM image of VO_2(B)/amorphous $SrTiO_3/SiO_2$ heterostructure on silicon substrate. (d) Magnified view of the interface between VO_2(B) and amorphous $SrTiO_3$. (e) Selected-area electron diffraction patterns of VO_2(B) and VO layers. (f) Schematic illustration of epitaxial VO_2(B) growth on amorphous $SrTiO_3$. Reproduced with permission from Ref. [73], © Elsevier Ltd. 2020.

fabrication and the thermal stability are improved by using an amorphous buffer layer.

5 Challenges and perspectives

In summary, we highlighted the importance of low-damage sputtering and introduced off-axis sputtering as a key approach for achieving high-quality epitaxial growth. Two distinct off-axis configurations, (1) 90° off-axis sputtering and (2) misaligned dual gun sputtering, are introduced. Misaligned dual-gun sputtering was proposed to increase the slow deposition rates associated with 90° off-axis sputtering. To illustrate the capabilities of low-damage sputtering for experiments requiring meticulous control, we discuss several critical cases: (1) thin films incorporating volatile elements, (2) superlattices that require precise regulation of each epitaxial interface, (3) real-time monitoring of epitaxial sputtering using RHEED, (4) anion doping to create oxynitride thin films, and (5) self-texturing and selective growth of specific polymorphic phases.

Low-damage sputtering, achieved by an off-axis configuration, can be a critical enabler for the "more than Moore" paradigm, which aims to push the boundaries of semiconductor devices by integrating diverse functionalities beyond traditional transistor scaling. This technique allows for the precise deposition of high-quality multifunctional thin films, making it ideal for applications requiring heterogeneous integration, such as sensors, optoelectronics, and quantum devices. Compared with other epitaxial deposition methods, sputtering offers several advantages: it is more cost-effective than molecular beam epitaxy (MBE), allows for more precise composition control in complex materials than chemical vapor deposition (CVD), supports larger-area deposition than pulsed laser deposition (PLD), and achieves higher growth rates than atomic layer deposition (ALD), facilitating the efficient creation of both thin and thick films. These unique strengths make low-damage sputtering particularly well-suited for fabricating complex, multi-functional devices required for the next generation of electronics. As semiconductor scaling reaches its limits, this technology provides the versatility and precision necessary to realize the "More than Moore" vision, enabling the incorporation of novel materials and functionalities into advanced device architectures.

Despite a long history of research on the synthesis of epitaxial complex oxide heterostructures and the discovery of novel physical phenomena, no commercial devices are currently available. As most oxide single-crystal substrates are much more expensive than Si, it is almost impossible to make commercial products from epitaxial heterostructures grown on an oxide single-crystal substrate, regardless of their excellent functional properties. For commercialization, it is essential to integrate high-quality epitaxial oxide thin films on Si. Recently, commercially available silicon wafers with epitaxial PZT/$SrRuO_3$/Pt/ZrO_2/Si structures have become available. Note that these commercial wafers are fabricated by a sputtering technique, which indicates that the sputtering method is commercially favorable for the epitaxial growth of complex oxide thin films compared with other deposition techniques, such as MBE, CVD, PLD, and ALD. However, owing to the large difference in chemical and physical properties between complex oxides and Si, it is difficult to directly grow high-quality thin films comparable to those on a single-crystal substrate. Additionally, the evolution of thermal stress originating from the large difference in the thermal expansion coefficient between oxides and Si is another critical problem. Recent advances in the epitaxy transfer technique can be a promising solution [75]; however, at present, the transfer process is not cost effective. Therefore, it is necessary to develop new epitaxial buffer layers on Si, the quality of which is much better than that of currently available CeO_2/YSZ buffer layers, using sputtering technique. However, achieving this goal appears to be challenging when conventional sputtering techniques are used.

Recently, hybrid deposition systems have emerged to synthesize higher-quality complex oxide thin films, enabling a level of precise controllability that is not achievable with conventional deposition techniques. For example, a CVD/MBE hybrid deposition technique was demonstrated, incorporating metal-organic (MO) precursors, typically used in the CVD process, into an MBE system [76]. Using effusion cells for Ba and Sr and an MO source of hexamethylditin (HMDT) for Sn, the hybrid-MBE technique allows precise control of the cation ratio to improve the carrier mobility, suppressing scattering events originating from defects such as vacancies, antisite defects, and off-stoichiometry. Additionally, a CVD/PLD hybrid deposition technique was demonstrated, utilizing a solid SrO ceramic target for PLD and a titanium tetraisopropoxide (TTIP) MO source for CVD [77]. This enables the growth of highly stoichiometric $SrTiO_3$ thin films with enhanced electron mobility. By harnessing the inherent versatility of sputtering techniques, the hybridization of sputtering with other deposition processes, especially with CVD-based methods, will present a promising pathway in both academic and industrial communities. This not only has the potential to propel advancements in film quality and subsequent material properties but also facilitates the synthesis of intricate heterostructures comprising a diverse array of materials, which are hitherto unattainable by conventional processes.

Hybrid systems, such as the combination of sputtering with CVD or ALD, allow for precise control over the stoichiometry of both cations and anions. Additionally, these methods can facilitate the creation of unique nanostructures, including nanowires, nanorods, columnar structures, and helical forms, which can be uniformly coated on their outer surfaces with heterogeneous materials. This capability increases the degree of freedom in thin film deposition, enabling the fabrication of complex material systems with tailored properties. However, challenges remain, including ensuring compatibility between deposition techniques, optimizing process conditions to prevent material degradation, and scaling these hybrid systems for industrial applications. Addressing these challenges will be essential for unlocking the full potential of hybrid thin-film deposition systems in future technological advancements.

With the advent of three-dimensional (3D) structured semiconductors, such as FinFET (short for fin field-effect transistor), a 3D transistor design characterized by its fin-like vertical structures that improve channel control and reduce power leakage in logic electronics, as well as 3D capacitors in dynamic random access memories (DRAMs), there is an increasing demand for the growth of epitaxial layers on 3D substrates. In general, a sputtering technique is considered conformal, ensuring that thin films adhere evenly to all surfaces, preventing gaps or uneven coverage that could impact the performance of electronic devices. Although the ability of conformal deposition in sputtering falls far behind that of ALD, it presents a new opportunity to explore 3D sputtering growth of epitaxial complex oxide thin films on trench or fin structures.

Finally, as a technical issue, it is worth emphasizing the issues of particle generation and contamination. Dust particles can evolve in a plasma during sputtering and fall onto the substrate, causing defects. Dust particles can be transported into the plasma from the

chamber walls, targets, and backsputtered substrates/heaters as flakes, causing detrimental effects on the quality and uniformity of thin films. Moreover, some plasma conditions can cause self-nucleation and subsequent growth of dust particles within the plasma, where deposition atoms and molecules are supersaturated. Instable plasma and high working pressure conditions are prone to increase the generation of dust particles. Appropriate mitigation strategies to suppress the detrimental effects of dust particles, such as optimizing sputtering parameters, chamber cleaning, or particle filters, should be further developed for commercialization.

Acknowledgements

The authors gratefully acknowledge the financial support from the National Research Foundation of Korea (NRF) grant funded by the Ministry of Science and ICT (No. NRF-2020M3D1A2101933) and from Korea Institute of Science and Technology (No. 2E33181). This work was also supported by Alchemist Project Program (No. RS-2024-00422061, Development of Ultimate Semiconductor by Control of Band Curvature of Ultra-wide Bandgap Materials) funded by the Ministry of Trade, Industry & Energy (MOTIE, Republic of Korea).

Declaration of competing interest

The authors have no competing interests to declare that are relevant to the content of this article.

References

[1] Waser R, Böttger U, Tiedke S. *Polar Oxides: Properties, Characterization, and Imaging*. New Jersey (USA): Wiley Online Library, 2005.
[2] Cox PA. *Transition Metal Oxides: An Introduction to Their Electronic Structure and Properties*. Oxford (UK): Oxford University Press, 2010.
[3] Maekawa S, Tohyama T, Barnes SE, *et al. Physics of Transition Metal Oxides*. Berlin (Germany): Springer, 2013
[4] Schlom DG, Chen LQ, Fennie CJ, *et al.* Elastic strain engineering of ferroic oxides. *MRS Bull* 2014, **39**: 118–130.
[5] Choi MJ, Lee JW, Jang HW. Strain engineering in perovskites: Mutual insight on oxides and halides. *Adv Mater* 2024, **36**: 2308827.
[6] Nataf GF, Guennou M, Gregg JM, *et al.* Domain-wall engineering and topological defects in ferroelectric and ferroelastic materials. *Nat Rev Phys* 2020, **2**: 634–648.
[7] Hwang HY, Iwasa Y, Kawasaki M, *et al.* Emergent phenomena at oxide interfaces. *Nat Mater* 2012, **11**: 103–113.
[8] Sun YL, Yang J, Li SA, *et al.* Defect engineering in perovskite oxide thin films. *Chem Commun* 2021, **57**: 8402–8420.
[9] Sarkar J. *Sputtering Materials for VLSI and Thin Film Devices*. Boston (USA): William Andrew Publishing, 2010: 291–491.
[10] Fraser DB. Sputter-deposited films for display devices. *Thin Solid Films* 1972, **13**: 407–412.
[11] Levy M, Osgood RM, Hegde H, *et al.* Integrated optical isolators with sputter-deposited thin-film magnets. *IEEE Photonics Technol Lett* 1996, **8**: 903–905.
[12] Smentkowski VS. Trends in sputtering. *Prog Surf Sci* 2000, **64**: 1–58.
[13] Park H, Lee S. Effect of sputter deposition on the adhesion and failure behavior between Cu film and glassy calcium aluminosilicate: A molecular dynamics study. *Metals* 2021, **11**: 1365.
[14] Baptista A, Silva FJG, Porteiro J, *et al.* On the physical vapour deposition (PVD): Evolution of magnetron sputtering processes for industrial applications. *Procedia Manuf* 2018, **17**: 746–757.
[15] Biersack JP, Santner E. Sputtering of potassium chloride by H, He, and Ar ions. *Nucl Instrum Meth* 1976, **132**: 229–235.
[16] Kon M, Song PK, Mitsui A, *et al.* Crystallinity of gallium-doped zinc oxide films deposited by DC magnetron sputtering using Ar, Ne or Kr gas. *Jpn J Appl Phys* 2002, **41**: 6174–6179.
[17] Grove WR. VII. On the electro–chemical polarity of gases. *Philos T R Soc Lond* 1852, **142**: 87–101.
[18] Greene JE. Review article: Tracing the recorded history of thin-film sputter deposition: From the 1800s to 2017. *J Vac Sci Technol A* 2017, **35**: 05C204.
[19] Kelly PJ, Arnell RD. Magnetron sputtering: A review of recent developments and applications. *Vacuum* 2000, **56**: 159–172.
[20] Berg S, Nyberg T. Fundamental understanding and modeling of reactive sputtering processes. *Thin Solid Films* 2005, **476**: 215–230.
[21] Chowdhury S, Laugier MT, Rahman IZ. Effect of target self-bias voltage on the mechanical properties of diamond-like carbon films deposited by RF magnetron sputtering. *Thin Solid Films* 2004, **468**: 149–154.
[22] Lamont LT Jr, Turner FT. The role of dc self-bias potential in the control of rf sputtering. *J Vac Sci Technol* 1974, **11**: 47–51.
[23] Hasan MM, Haseeb ASMA, Saidur R, *et al.* Influence of substrate and annealing temperatures on optical properties of RF-sputtered TiO_2 thin films. *Opt Mater* 2010, **32**: 690–695.
[24] Raj PD, Gupta S, Sridharan M. Nanostructured V_2O_5 thin films deposited at low sputtering power. *Mater Sci Semicond Process* 2015, **39**: 426–432.
[25] Hones P, Sanjines R, Levy F. Characterization of sputter-deposited chromium nitride thin films for hard coatings. *Surf Coat Tech* 1997, **94**: 398–402.
[26] Izyumskaya N, Avrutin V, Ding K, *et al.* Emergence of high quality sputtered III-nitride semiconductors and devices. *Semicond Sci Technol* 2019, **34**: 093003.
[27] Pleskunov P, Košutová T, Vaidulych M, *et al.* The sputter-based synthesis of tantalum oxynitride nanoparticles with architecture and bandgap controlled by design. *Appl Surf Sci* 2021, **559**: 149974.
[28] Hegedüs N, Balázsi C, Kolonits T, *et al.* Investigation of the RF sputtering process and the properties of deposited silicon oxynitride layers under varying reactive gas conditions. *Materials* 2022, **15**: 6313.
[29] Jansson U, Lewin E. Sputter deposition of transition-metal carbide films—A critical review from a chemical perspective. *Thin Solid Films* 2013, **536**: 1–24.
[30] Larhlimi H, Ghailane A, Makha M, *et al.* Magnetron sputtered titanium carbide-based coatings: A review of science and technology. *Vacuum* 2022, **197**: 110853.
[31] Iqbal A, Mohd-Yasin F. Reactive sputtering of aluminum nitride (002) thin films for piezoelectric applications: A review. *Sensors* 2018, **18**: 1797.
[32] Manova D, Gerlach JW, Mändl S. Thin film deposition using energetic ions. *Materials* 2010, **3**: 4109–4141.
[33] Taga Y, Takahasi R. Role of kinetic energy of sputtered particles in thin film formation. *Surf Sci* 1997, **386**: 231–240.
[34] Stangeby PC. The plasma sheath. In: *Physics of Plasma–Wall Interactions in Controlled Fusion*. Post DE, Behrisch R, Eds. Boston (USA): Springer US, 1986: 41–97.
[35] Carcia PF, McLean RS, Reilly MH, *et al.* Influence of energetic bombardment on stress, resistivity, and microstructure of indium tin oxide films grown by radio frequency magnetron sputtering on flexible polyester substrates. *J Vac Sci Technol A* 2003, **21**: 745–751.
[36] Aydin E, Altinkaya C, Smirnov Y, *et al.* Sputtered transparent electrodes for optoelectronic devices: Induced damage and mitigation strategies. *Matter* 2021, **4**: 3549–3584.
[37] Baptista A, Silva F, Porteiro J, *et al.* Sputtering physical vapour deposition (PVD) coatings: A critical review on process improvement and market trend demands. *Coatings* 2018, **8**: 402.
[38] Martin PM. *Handbook of Deposition Technologies for Films and Coatings: Science, Applications and Technology*. New York (USA): William Andrew Publishing, 2009: 21–22.
[39] Eom CB, Sun JZ, Lairson BM, *et al.* Synthesis and properties of $YBa_2Cu_3O_7$ thin films grown *in situ* by 90° off-axis single magnetron sputtering. *Phys C Supercond* 1990, **171**: 354–383.

[40] Rao RA, Gan Q, Eom CB, *et al.* Uniform deposition of $YBa_2Cu_3O_7$ thin films over an 8 inch diameter area by a 90° off-axis sputtering technique. *Appl Phys Lett* 1996, **69**: 3911–3913.
[41] Podkaminer JP, Hernandez T, Huang M, *et al.* Creation of a two-dimensional electron gas and conductivity switching of nanowires at the $LaAlO_3/SrTiO_3$ interface grown by 90° off-axis sputtering. *Appl Phys Lett* 2013, **103**: 071604.
[42] Brewer A, Cho KH, Saenrang W, *et al.* Uniform sputter deposition of high-quality epitaxial complex oxide thin films. *J Vac Sci Technol A* 2017, **35**: 060607.
[43] Radzimski ZJ, Posadowski WM, Rossnagel SM, *et al.* Directional copper deposition using dc magnetron self-sputtering. *J Vac Sci Technol B* 1998, **16**: 1102–1106.
[44] Balmuchu SP, Sahu S, Dobbidi P. Enhanced magnetic properties and leakage current mechanism in bismuth lanthanum ferrite thin films coupled with impedance and magnetic studies. *Vacuum* 2023, **215**: 112356.
[45] Bernstein SD, Wong TY, Collins SR, *et al.* Effects of excess Pb on crystallization and electrical properties of ferroelectric PZT films deposited by reactive RF magnetron sputtering. *MRS Online Proc Libr* 1994, **361**: 477–482.
[46] Kwo J, Fleming R, Kao H, *et al.* Single domain high T_C $La_{2-x}Sr_xCuO_4$ films with tilted CuO_2 planes. *Appl Phys Lett* 1992, **60**: 1905–1907.
[47] Eom CB, Cava RJ, Fleming RM, *et al.* Single-crystal epitaxial thin films of the isotropic metallic oxides $Sr_{1-x}Ca_xRuO_3$ ($0 \le x \le 1$). *Science* 1992, **258**: 1766–1769.
[48] Pohl UW. *Epitaxy of Semiconductors: Physics and Fabrication of Heterostructures*. Berlin (Germany): Springer, 2020: 268–269.
[49] Baek SH, Park J, Kim DM, *et al.* Giant piezoelectricity on Si for hyperactive MEMS. *Science* 2011, **334**: 958–961.
[50] Shepard JF, Moses PJ, Trolier-McKinstry S. The wafer flexure technique for the determination of the transverse piezoelectric coefficient (d_{31}) of PZT thin films. *Sens Actuat A Phys* 1998, **71**: 133–138.
[51] Baek SH, Jang HW, Folkman CM, *et al.* Ferroelastic switching for nanoscale non-volatile magnetoelectric devices. *Nat Mater* 2010, **9**: 309–314.
[52] Jang HW, Ortiz D, Baek SH, *et al.* Domain engineering for enhanced ferroelectric properties of epitaxial (001)BiFeO thin films. *Adv Mater* 2009, **21**: 817–823.
[53] Chu YH, Cruz M , Yang CH, *et al.* Domain control in multiferroic $BiFeO_3$ through substrate vicinality. *Adv Mater* 2007, **19**: 2662–2666.
[54] Seidel J, Martin LW, He Q, *et al.* Conduction at domain walls in oxide multiferroics. *Nat Mater* 2009, **8**: 229–234.
[55] Farokhipoor S, Noheda B. Conduction through 71° domain walls in $BiFeO_3$ thin films. *Phys Rev Lett* 2011, **107**: 127601.
[56] Baek SH, Folkman CM, Park JW, *et al.* The nature of polarization fatigue in $BiFeO_3$. *Adv Mater* 2011, **23**: 1621–1625.
[57] Tsai HN, Liang YC, Lee HY. Characteristics of sputter-deposited $BaTiO_3/SrTiO_3$ artificial superlattice films on a $LaNiO_3$-coated $SrTiO_3$ substrate. *J Cryst Growth* 2005, **284**: 65–72.
[58] Kanno I, Hayashi S, Takayama R, *et al.* Superlattices of $PbZrO^3$ and $PbTiO_3$ prepared by multi-ion-beam sputtering. *Appl Phys Lett* 1996, **68**: 328–330.
[59] Ravichandran J, Yadav AK, Cheaito R, *et al.* Crossover from incoherent to coherent phonon scattering in epitaxial oxide superlattices. *Nat Mater* 2014, **13**: 168–172.
[60] Zurbuchen MA, Podraza NJ, Schubert J, *et al.* Synthesis of the superlattice complex oxide $Sr_5Bi_4Ti_8O_{27}$ and its band gap behavior. *Appl Phys Lett* 2012, **100**: 223109.
[61] Moetakef P, Cain TA, Ouellette DG, *et al.* Electrostatic carrier doping of $GdTiO_3/SrTiO_3$ interfaces. *Appl Phys Lett* 2011, **99**: 232116.
[62] Disa AS, Georgescu AB, Hart JL, *et al.* Control of hidden ground-state order in $NdNiO_3$ superlattices. *Phys Rev Materials* 2017, **1**: 024410.
[63] Dawber M, Stucki N, Lichtensteiger C, *et al.* Tailoring the properties of artificially layered ferroelectric superlattices. *Adv Mater* 2007, **19**: 4153–4159.
[64] Ohtomo A, Hwang HY. A high-mobility electron gas at the $LaAlO_3/SrTiO_3$ heterointerface. *Nature* 2004, **427**: 423–426.
[65] Singh-Bhalla G, Bell C, Ravichandran J, *et al.* Built-in and induced polarization across $LaAlO_3/SrTiO_3$ heterojunctions. *Nat Phys* 2011, **7**: 80–86.
[66] Kalisky B, Bert JA, Klopfer BB, *et al.* Critical thickness for ferromagnetism in $LaAlO_3/SrTiO_3$ heterostructures. *Nat Commun* 2012, **3**: 922.
[67] Podkaminer JP, Patzner JJ, Davidson BA, *et al.* Real-time and *in situ* monitoring of sputter deposition with RHEED for atomic layer controlled growth. *APL Mater* 2016, **4**: 086111.
[68] Meng WJ, Heremans J, Cheng YT. Epitaxial growth of aluminum nitride on Si(111) by reactive sputtering. *Appl Phys Lett* 1991, **59**: 2097–2099.
[69] Li P, Jiang EY, Bai HL. Fabrication of ultrathin epitaxial γ-Fe_2O_3 films by reactive sputtering. *J Phys D: Appl Phys* 2011, **44**: 075003.
[70] Jeong BS, Budai JD, Norton DP. Epitaxial stabilization of single crystal anatase films via reactive sputter deposition. *Thin Solid Films* 2002, **422**: 166–169.
[71] Fang YS, Do TH, Chiu KA, *et al.* Reactive sputtering deposition of epitaxial TiC film on Si(100) substrate. *Coatings* 2020, **10**: 647.
[72] Gwon HJ, Kang NR, Lee YJ, *et al.* Enhancement of mechanical hardness in SnO_xN_y with a dense high-pressure cubic phase of SnO_2. *Chem Mater* 2016, **28**: 7051–7057.
[73] Kil TH, Choi HJ, Lee G, *et al.* Selective growth and texturing of VO_2(B) thin films for high-temperature microbolometers. *J Eur Ceram Soc* 2020, **40**: 5582–5588.
[74] Lee HJ, Wang D, Kim TH, *et al.* Wide-temperature (up to 100 °C) operation of thermostable vanadium oxide based microbolometers with Ti/MgF_2 infrared absorbing layer for long wavelength infrared (LWIR) detection. *Appl Surf Sci* 2021, **547**: 149142.
[75] Ji J, Park S, Do H, *et al.* A review on recent advances in fabricating freestanding single-crystalline complex-oxide membranes and its applications. *Phys Scr* 2023, **98**: 052002.
[76] Nunn W, Truttmann TK, Jalan B. A review of molecular-beam epitaxy of wide bandgap complex oxide semiconductors. *J Mater Res* 2021, **36**: 4846–4864.
[77] MacManus-Driscoll JL, Wells MP, Yun C, *et al.* New approaches for achieving more perfect transition metal oxide thin films. *APL Mater* 2020, **8**: 040904.